Thermal Characteristic Evaluation of Functionally Graded Composites for PSZ/Metal

Jae Kyoo Lim*
The Research Institute of Industrial Technology, Chonbuk National University
Jun Hee Song
Automobile High-Technology Research Institute, Chonbuk National University

The functionally graded material (FGM) is the new concept for a heat resisting material. FGM consists of ceramics on one side and metal on the other. A composition and microstructure of an intermediate layer change continuously from ceramics to metal at the micron level. This study is carried out to analyze the thermal shock characteristics of functionally graded PSZ/metal composites. Heat-resistant property was evaluated by gas burner heating test using C_2H_2/O_2 combustion flame. The ceramic surface was heated with burner flame and the bottom surface cooled with water flow. Also, the composition profile and the thickness of the graded layer were varied to study the thermomechanical response. Furthermore, this study carried out the thermal stress analysis to investigate the thermal characteristics by the finite element method. Acoustic emission (AE) monitoring was performed to detect the microfracture process in a thermal shock test.

Key Words: Functionally Graded Material, Thermal Shock, Thermal Stress, Gas Burner Heating, Acoustic Emission

1. Introduction

Development of a new material is required for use in the severe environment. Functionally Graded Material (FGM) consists of a new material design to make intentionally irregular dispersion state (Niino, 1990). A component density and quality of FGM are varied continuously from place to place (Watanabe, 1993). The FGM could possess multiple properties simultaneously to withstand severe heating and oxidation environments with steep temperature gradient. In developing a new material, the material evaluation part is very important with design and process parts of suitable one's system. In the heat-resistant thermal shock evaluation of FGM (Gill, 1986 ; Miller, 1987) before performance evaluation in large-scale is performed, an imitation test for small specimen is necessary. For such a characteristic test, several heating methods have been developed using furnace, laser and plasma arc, etc. (Miyawaki 1990 ; Kumakawa, 1990 ; Song, 1996). A local heating test with a gas burner is one of these and the effective method that can simulate the high thermal environment such as the wall of combustion chamber with a thrust unit like in a space plane.

In this study, the local heating test (i. e., thermal shock test) with a gas burner was carried out to simulate the thermal environment of the severe condition in ceramic/metal FGM. We evaluated the fracture resistance of thermal shock under steady-state and FGM varies with composition structure to examine the effect of the composition profile (Kawasaki 1987). Furthermore, AE monitoring was performed to detect the microfracture process during the thermal shock test by

* Corresponding Author,
E-mail : jklim@moak. chonbuk. ac. kr
TEL : +82-652-270-2321 ; **FAX** : +82-652-270-2460
Faculty of Mechanical Engineering, The Research Institute of Industrial Technology, Chonbuk National University, Chonju 561-756, Korea. (Manuscript **Received** April 27, 1999 ; **Revised** December 1, 1999)

the gas burner and the thermal stress analysis was theoretically conducted using a FEM program. The fracture surfaces were examined by scanning electron microscopy (SEM).

2. Specimen and Test Methods

2.1 Specimen

The samples used in the thermal shock test and thermal stress analysis were respectively the disk-shaped and the cylindrical PSZ/metal composites of FGM and NFGM (non-FGM, the conventional ceramic/metal composites). Figure 1 shows the size and geometry of the disk-shaped specimen. The coating layers were plasma sprayed with NiCrAlY and ZrO_2-8wt%Y_2O_3 (PSZ) on stainless steel substrate. In the specimen of T-type disk the diameter of surface part heated was 14mm. In the cross section observation, no defects such as large residual pores or small cracks are observed on the sample.

The cylindrical shape of specimen simulated the curvature of the leading edge of a gas turbine blade and its dimension and composition were shown in Fig. 2. As shown in the figure, the outer diameter of substrate was 8mm and thickness was 2mm. In FGM, the graded layer of ceramics (PSZ) and the bond coat (NiCrAlY) was 0.75mm thick. NFGM consisted of the ceramic coating layer of 0.35mm thick and NiCrAlY of 0.15mm thick. The coating layers were plasma sprayed with NiCrAlY and PSZ on stainless steel substrate.

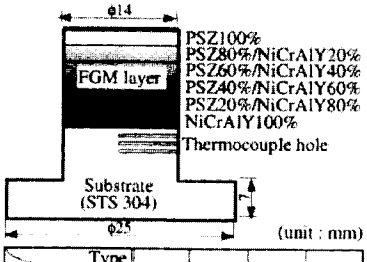

Composition \ Type	NFGM	FGM1	FGM2	FGM3
PSZ 100%	0.35	0.31	0.19	0.11
PSZ 80%/ NiCrAlY 20%		0.19	0.19	0.12
PSZ 60%/ NiCrAlY 40%		0.09	0.19	0.15
PSZ 40%/ NiCrAlY 60%		0.05	0.19	0.21
PSZ 20%/ NiCrAlY 80%			0.24	0.96
NiCrAlY 100%	0.10	0.10	0.10	0.10

※ PSZ: ZrO_2-8wt%Y_2O_3

Fig. 1 Specification of thermal shock specimen by a gas burner

2.2 Burner heating apparatus

Figure 3 shows a schematic diagram of the experimental set-up for the gas burner heating on a laboratory scale. The heating source was used with oxygen and acetylene gas. The top surface temperature of the specimen was measured using a emission thermometer and cooling condition of the bottom surface. Thermocouples with 0.5mm diameter were inserted into three holes drilled through the substrate 3mm apart. AE sensor was attached on the holder of the specimen grip.

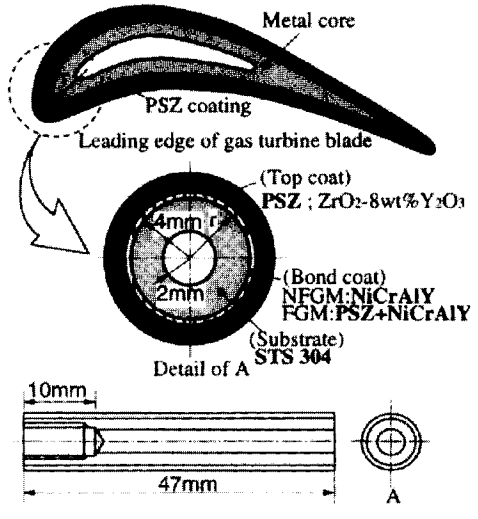

Fig. 2 Specimen model of the cylindrical type

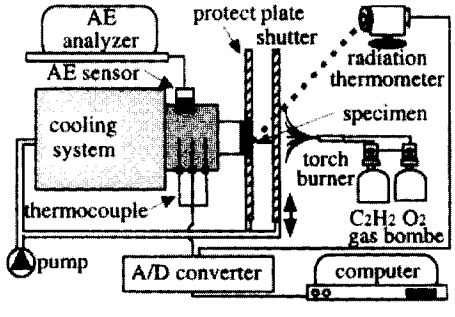

Fig. 3 Gas burner test system

2.3 AE test

AE monitoring was carried out using LOCAN AT ANALYZER made by Physical Acoustic Co.. The detected signals were amplified with a gain of 40dB in the preamplifier and filtered through 100~1200kHz bandpass filter to reduce the background noise and then fed to the AE analyzer. The AE electrical signals were amplified again with 40dB in the main amplifier and analyzed using the A/D converter for signal processing. The threshold level for AE monitoring was set just above the background noises. Total gain and threshold level were respectively 80dB and 40dB. Because of test conditions of high temperatures, the grip holder was used as the wave guide. Also, the AE energy parameter was the measured area under the rectified signal envelop and was responsive to both amplitude and duration of the event. AE energy was stored in 'dB'.

2.4 FEM analysis

The thermal stress calculation was conducted using the MARC program. The model was dealt with a 2-dimensional axisymetric problem, the element was rectangular. As shown in Fig. 4, X-coordinates was rotating axis and Y-coordinates indicated the radial direction. In the case of NFGM and FGM, 180, 330 elements and 209, 374 nodes were used, respectively. However, since the ceramic coating layer was easily broken under the thermal stress, to evaluate a practical application of FGM it would be the most important to clarify the stress state of interface including ceramic part (Miller 1982).

Hence the mesh generation was densely divided at the interface. Table 1 summarizes the mechanical properties used in the calculation (Batakis 1984; Chung 1985). Also, the temperature-dependent material properties were considered in this analysis.

After these materials were heated from a room temperature to the maximum temperature, then the FEM analysis was used to investigate the residual stresses developed during the cooling from the maximum temperature to a room temperature. Thermal stress distributions in the process of cooling were determined under the steady state. Also, the analysis results were obtained as the distribution of residual stress parameters, that was axial stress (σa), radial stress (σr), hoop stress (σh), and shear stress (τra). In the case of NFGM, the maximum temperatures were 700℃, 800℃, 900℃ and 1000℃, and that of FGM were

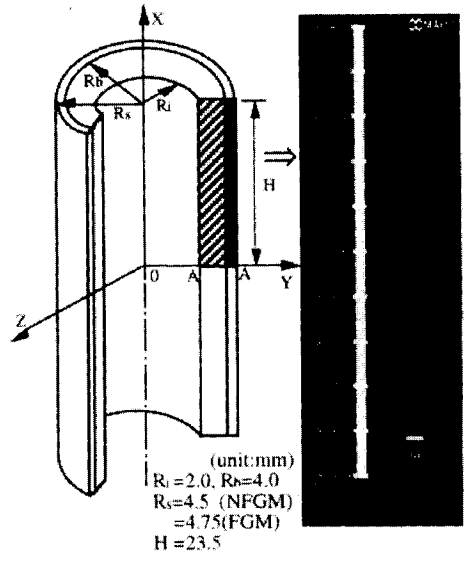

Fig. 4 The FEM model of thermal stress analysis

Table 1 Thermal and mechanical properties used in finite-element analysis

Material	Young's modulus E(GPa)	Thermal expansion Co. $\alpha(\times 10^{-6}/℃)$	Poisson ratio μ
PSZ	E=45.06−0.0248T ; T in ℃	100℃ − 9.75 600℃ − 10.9 400℃ − 10.7 1000℃ − 10.7	0.23
NiCrAlY	E=125.06−0.0149T ; T in ℃	100℃ − 12.5 600℃ − 15.7 400℃ − 14.3 1000℃ − 16.5	0.23
STS304	E=201.44−0.1643T ; T in ℃	100℃ − 17.3 400℃ − 17.9 600℃ − 18.7 1000℃ − 20.6	0.29

NFGM conditions added to 1100℃.

3. Test Results and Discussion

3.1 Thermal shock behavior

Thermal shock procedure by a gas burner was conducted to the three thermal steps of heating, holding and cooling in a specific temperature condition. Temperature distributions at the sample surface were measured with the emission thermometer which could detect the temperature range from 600℃ to 3000℃ in a steady-state heating condition. The surface temperature is higher in the central part than those at the specimen edge, decreasing inversely with the radial distance. The specimen surface temperature was uniform over a diameter of about 3㎜ from the center. The temperature of the central part of the specimen surface was nominally called as the surface temperature in the present data.

The heating time is about 2 and 3 minutes up to the maximum temperature of about 1000 and 1100℃. This is increased with the maximum temperature. Due to their similar tendency, the only condition of 3min. at 1100℃ will be explained in this paper. The surface(Ts)/bottom(Tb) temperature and AE energy distribution were indicated by the solid line/dashed line and histogram respectively in the figures.

Figure 5 shows the temperature distribution and AE energy behavior in NFGM. As soon as the surface temperature was increased up to 1089℃, this was rapidly cooled to room temperature. Also, the bottom temperature was distributed with similar response. Then, the temperature difference was 444℃. The majority of the AE activity took place during the cooling step rather than the heating step. The AE energy was more detected with the cooling time. The total AE energy was 87,683dB and the maximum AE energy was 2,389dB at bottom temperature of 50℃.

Figure 6 shows the temperature distribution and AE energy behavior in FGM1 of which the compositional profile is convex(P=1/3). The surface temperature was increased up to 1107℃. Then, the temperature difference was 527℃. AE behavior shown more emission frequency in FGM1 than NFGM and mainly occurred on cooling. There was relatively less emission of below 500dB during cooling up to 300℃, but AE energy was more detected with the cooling time. The total AE energy was 69,485dB and the maximum AE energy was 1,625dB at bottom temperature of 157℃.

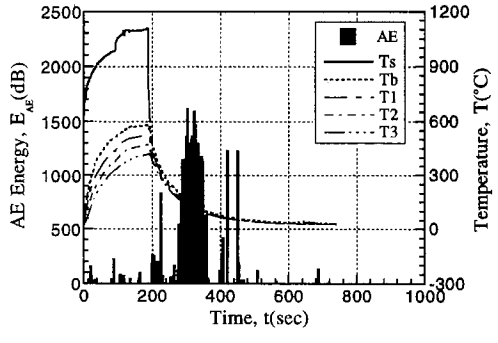

Fig. 6 AE behavior and temperature history by burner heating in FGM1

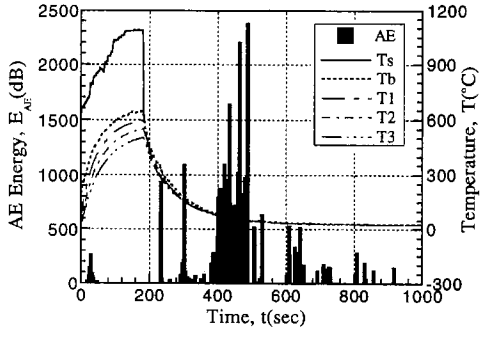

Fig. 5 AE behavior and temperature history by burner heating in NFGM

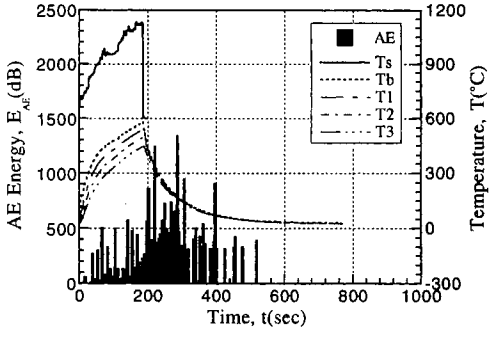

Fig. 7 AE behavior and temperature history by burner heating in FGM2

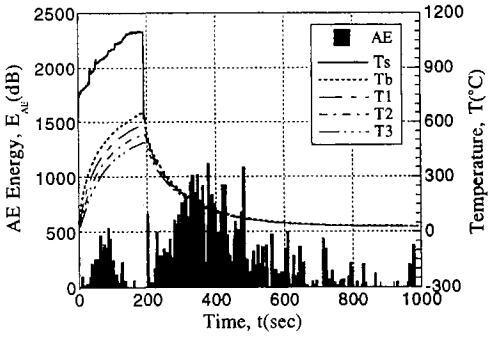

Fig. 8 AE behavior and temperature history by burner heating in FGM3

Figure 7 shows the temperature distribution and AE energy behavior in FGM2 of which the compositional profile is linear(P=1). The maximum surface temperature was 1133℃. Then, the temperature difference was 556℃. The total AE energy was 85,862dB and the maximum AE energy was 1,342dB at bottom temperature of 174℃.

Figure 8 shows the temperature distribution and AE energy behavior in FGM3 of which the compositional profile is concave(P=3). The maximum surface temperature was 1101℃. Then, the temperature difference was 450℃. The total AE energy was 155,530dB and the maximum AE energy was 1,119dB at bottom temperature of 132℃.

Therefore, the heat-resistant characteristic can be examined by thermal history and AE behavior condition for thermal shock test. The size of the maximum AE energy under the direct influence of fracture is arranged in order of NFGM>FGM1 >FGM2>FGM3. Namely, NFGM showed the most fragile property in thermal shock due to the largest occurrence of the maximum AE energy. On the other hand FGM3 shows the highest heat-resisting performance among these specimens. Because FGM was provided with the function of mitigating the induced thermal stress by the graded layers, it could be confirmed that FGM was more superior than NFGM for the thermal shock resistance.

3.2 Fracture surface observation

Figure 9 is the SEM photographes that are

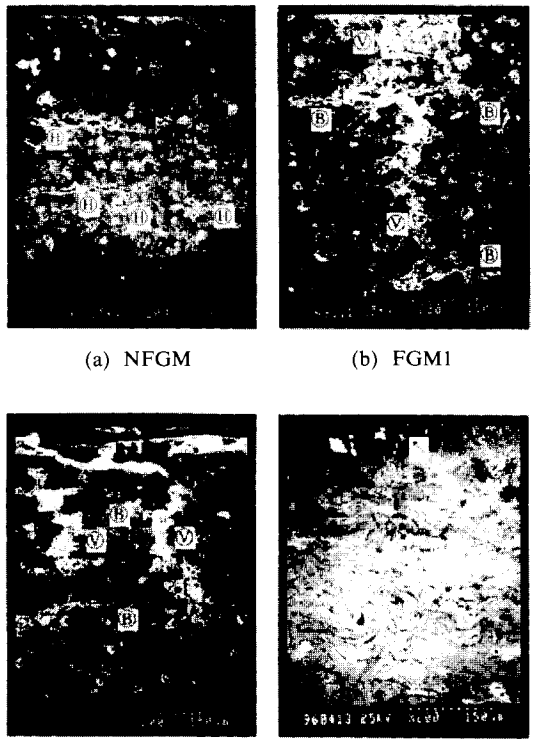

(a) NFGM (b) FGM1

(c) FGM2 (d) FGM3

Fig. 9 Photographs of fracture surface by gas burner thermal shock test

observed in a section of specimen after the thermal shock test. In Fig. 9(a) NFGM, the several horizontal cracks(Ⓗ) were observed in the middle of ceramics layer. Fracture level was the large-scale extending to degree of spallation. In Fig. 9(b) of FGM1, the vertical crack(Ⓥ) and the branch crack(Ⓑ) were also observed. In Fig. 9(c) of FGM2, the vertical crack(Ⓥ) and the branch crack(Ⓑ) were also observed. In Fig. 9 (d) of FGM3, the small-scale cracks(↖) were formed only at PSZ 100% layer and a large crack (i. e., delamination or spallation) wasn't found in all fracture surface. This fracture level was the highest in NFGM and the lowest in FGM3.

The effect of test temperature on the maximum AE energy distribution is presented in Fig. 10. The distribution of the maximum AE energy level is NFGM>FGM1>FGM2>FGM3. In the correlation between fracture surface observation and AE behavior, if the maximum AE energy level is above 1100dB approximately, it was obtained

information of onset of the material failure. The results of all fracture surface observation are identical with the AE analyses. The AE technique is to support the effective method in detection of microfracture process.

3.3 FEM analysis

Figure 11 shows residual stress distribution in ceramic part of NFGM with temperature conditions. The radial stress shows the tensile stress and the compressive stress is increased in order of shear stress, hoop stress and axial stress. With increase of temperature, the compressive stress increased in the axial stress, the hoop stress and the shear stress, but the tensile stress increased in the radial stress, gradually. Because the ceramic part is easy to break from the tensile stress, the more such radial stress increase, the more it is likely to lead to the failure of material. The radial stress in the ceramic part is given in Fig. 12. The solid line and the dashed line indicate the maximum and the mean stress. As shown in figure, both the maximum and the mean radial stress show the increase in the tensile stress with temperature. Also, the maximum radial stress was distributed with the tensile stress of 100MPa and over. What is more important is the fact that the increasing rate of residual stress is on the decrease to start at 800℃. It was considered that an energy release would be occurred at 800℃ condition. That is, it could be known that a crack of the material was caused by the radial stress. Therefore, it can be inferred that delamination in interface will be formed by the radial stress developed in ceramic part because the interface of ceramic (PSZ) and bond coat(NiCrAlY) is the most fragile.

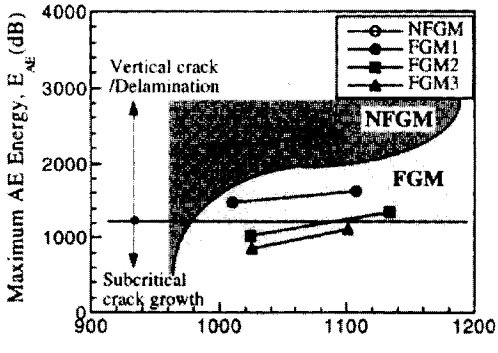

Fig. 10 Fracture condition for thermal shock

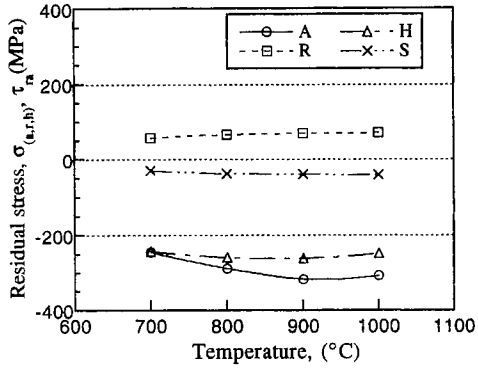

Fig. 11 Residual stress in PSZ part of NFGM

Figure 13(a) and (b) show the residual stress distribution of the maximum and the minimum stress with temperature in FGM. In the PSZ part, the stresses are indicated by '○◇□△' sign and stresses of the gradient layer, PSZ+NiCrAlY, are shown by '●◆■▲' sign. In Fig. 13(a), the maximum stresses were distributed with the largest shear stress of above 30MPa in PSZ part and the radial stress of above 24MPa. In Fig. 13 (b), the minimum stress were similar order of the maximum stress distribution and all stresses were subjected in the compressive stress.

Figure 14(a) and (b) show the axial and the shear stress distribution with temperature in PSZ part of FGM. The axial stress of '○' sign was increased in the compressive stress of over 245MPa.

However, the compressive stress for the axial

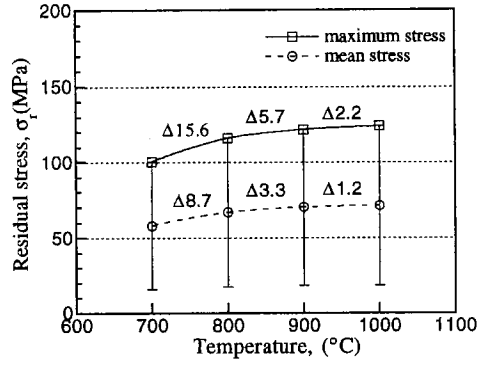

Fig. 12 Residual stress variation in PSZ part of NFGM

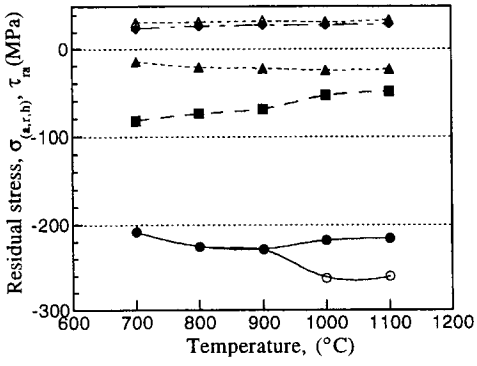

(a) Maximum stress

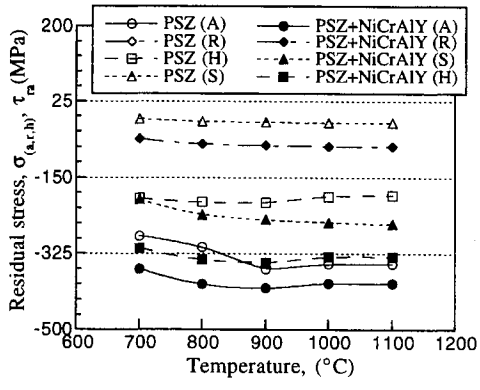

(b) Minimum stress

Fig. 13 Residual stress in PSZ and graded layer part of FGM

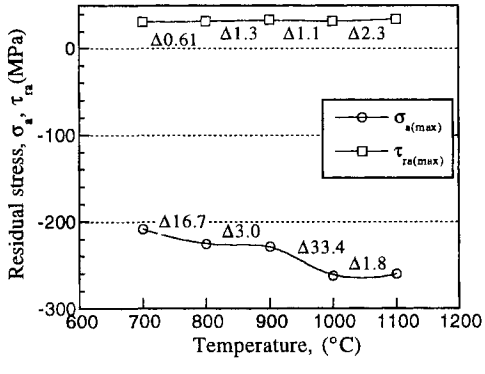

Fig. 14 Residual stress variation in PSZ part and graded layer of FGM

stress at the vicinity of 1000℃ has a tendency to increase with a large slope. Also, the shear stress of '□' sign has shown a similar characteristic of the axial stress and was decreased at 1000℃. This means that energy release was occurred at 1000℃ condition and that was, it could be known that the material would be damaged by such thermal stress. Judging from distribution characteristic of the axial and the shear stress, it is inferred that the vertical crack will be formed in ceramic part.

Consider the stress state and fracture mechanism occurred during the thermal shock test. Here the object is narrowed down to ceramic part because the vicinity of ceramic with top-coat is the most weak. There are in the state of 2-axial compressive stress on heating, but the tensile stress is acted by cooling. Due to the tensile stress, the crack initiated and propagated from the surface. Crack coalescence occurs and finally material is damaged. However, the shape of fracture is different with the direction of the applied stress. The radial stress parallel with thickness direction of coating layer occurs delamination in the interface which cohesion of heterogeneous material is weak. But, The axial stress perpendicular to thickness induces the vertical crack in ceramic part which mechanical property is low. That is, fracture mechanism can be inferred with characteristic of the residual stress.

4. Conclusions

In this stduy, the fracture behaviors of NFGM and FGM were analyzed and evaluated by the thermal shock test and thermal stress analysis under the high temperature atmosphere. The results obtained in this study can be summarized as belows ;

(1) NFGM couldn't be used in the thermal shock condition of above 1000℃, but FGM was still integrated in 1100℃ condition. Also, FGM3 showed the highest heat-resisting performance.

(2) NFGM was damaged as the vertical crack and delamination, but delamination fracture wasn't observed in FGMs. Because the graded layers in FGM mitigated the induced thermal stress, FGM was more superior than NFGM for the thermal shock resistance.

(3) AE behaviors were accorded with fracture characteristics and then AE technique was the effective evaluation method in thermal shock test. The gas burner test was effective in thermal shock

method that could be supported high thermal environment as a small specimen.

(4) In thermal stress analysis, fracture mechanism can be inferred that delamination is formed at 800℃ in NFGM but the vertical crack is occurred at 1000℃ in FGM. This results of thermal shock test and thermal stress analysis are identical.

References

Batakis, A.P. and Vogen, J.W., 1984, "Rocket Thrust Chamber Thermal Barrier Coatings," *NASA-CR-175022*.

Chung, B.T.F. and Kermanl, M.M. et al., 1985. "Heat Transfer in Thermal Barrier Coated Rods with Circumferential and Radial Temperature Gradient," *Journal Eng. Gas Turbine Power*, 107. pp. 135~141.

Gill, B.J. and Tucker, R.C.Jr., 1986, "Plasma Spray Coating Processes," *Mater. Sci. Tech.*, Vol. 2, pp. 207~213.

Kawasaki, A. and Watanabe, R., 1987, "Finite Element Analysis of Thermal Stress of the Metal/Ceramic Multi-Layer Composites with Controlled Compositional Gradients," *Journal Japan Inst. Metals*, Vol. 51, No. 6, pp. 525~529.

Kumakawa, A., Sasaki, M., Maeda, S. and Adachi, N., 1990. "Evaluation on Thermomechanical Properties of Functionally Gradient materials with High Temperature Gradients," *Journal of the Japan Soc. of Powder & Powder Metallurgy*, Vol. 37, No. 2, pp. 313~316.

Miller, R.A., 1987, "Current Status of Thermal Barrier Coatings," *Sur. & Coat. Tech.*, Vol. 30, pp. 1~11.

Miller, R.A. and Lowell, C.E. 1982, "Failure Mechanisms of Thermal Barrier Coatings Exposed to Elevated Temperatures," *Thin Solid Films*, 95, pp. 265~273.

Miyawaki, K., Hashida, T. and Takahashi, H., 1990, "Study on Evaluation of Thermal Shock Fracture and Thermal Stress Relaxation Property of FGM by Laser Local Heating Technique," *Journal of the Japan Soc. of Powder & Powder Metallurgy*, Vol. 37, No. 7, pp. 957~961.

Niino, M., 1990, "Development of Functionally Gradient material," *Journal of the Japan Soc. of Powder & Powder Metallurgy*, Vol. 37, No. 2, pp. 241~244.

Song, J.H., Lim, J.K. and Takahashi, H., 1996, "Thermal Shock/Fatigue Evaluation of FGM by AE Technique," *KSME Int. Journal*, Vol. 10, No. 4, pp. 435~442.

Watanabe, R., 1993, "Functionally Gradient Material," *FGM Research Group and The Society of Non-traditional Tech.*, pp. 306~310.